PCCP

PAPER



Cite this: *Phys. Chem. Chem. Phys.*, 2017, **19**, 20559

# How side chains affect conformation and electrical properties of poly(acrylic acid) in solution?

Xinlu Zhou and Kongshuang Zhao *

Received 15th April 2017,
Accepted 6th July 2017

DOI: 10.1039/c7cp02460f

rsc.li/pccp

To better understand the effect of side chains on the chain conformation and electrical properties of polyelectrolytes, dielectric measurements were carried out on solutions of poly(acrylic acid) (PAA), poly(acrylic acid)-*graft*-dodecyl (PAA-*g*-dodecyl), and poly(acrylic acid)-*graft*-poly(ethylene oxide) (PAA-*g*-PEO) over a wide concentration range. Double dielectric relaxations with counterion distribution were observed for these polymers and a refined double-layer polarization model was proposed to analyze these, by which valuable information about conformations and interfacial electrokinetic properties was obtained. The transitional concentrations for the overlapping and entanglement of chains were identified from results for the dielectric increment and relaxation time. The concentration dependences of the ratio of effective charges were estimated from conductivity data. It was shown that effective charges on PAA were greatly influenced by PEO or dodecyl side chains, which caused steric hindrance of counterion binding and further dissociation of carboxylic groups or bound counterions. Moreover, a mutual superposition and offsetting effect of PEO and dodecyl side chains was observed. An enhancement in the interpenetration of counterion atmospheres as a result of side chains was also found. In addition, the rate constant ratio and the distance of counterion fluctuations perpendicular to the chains were estimated. It was demonstrated that the effects of side chains on the effective charges or ionization properties of GCP play an important role in their conformation, counterion distribution, and fluctuation.

## 1. Introduction

Water-soluble graft copolymers (GCPs) form a major class of polymeric systems that are composed of a main chain and one or more chemically distinct side chains.[1] They spontaneously form inter- or intramolecular aggregates in aqueous solution owing to various association interactions induced by the side chains.[2] When the main chains or side chains are charged, a GCP will exhibit some features of polyelectrolytes (PEs), namely, viscoelasticity and conductivity.[3] These endow GCPs with a wide range of applications in the fields of biochemistry[4] and industry.[5,6] An understanding of their unique structure and properties in solution is needed for the design of desired GCPs and the prediction of their behavior in solution. Therefore, a relevant fundamental issue, namely, the effect of branching on the evolution of the conformation and electrical properties of chains, has excited wide interest in the fields of polymer science and soft condensed matter physics.

The morphology and flexibility of chains have been widely studied for GCPs with different densities,[7–9] distributions,[10] lengths[11] and chemical compositions[12] of side chains, whereby the effects of side chains on chain stiffness or various non-coulombic interactions such as hydrogen bonding and hydrophobic interactions have been confirmed. However, the abovementioned studies almost ignored the effect of side chains on effective charges and the condensation/release behavior of counterions. In general, abrupt collapse occurs owing to counterion condensation and electrostatic shielding from excess ions in the case of additive electrolytes.[13] Therefore, it is necessary to reconsider the effective charges or ionization properties of GCPs to better understand the effect of side chains on their structure and properties in solution.

In fact, the effects of side chains on effective charges or ionization properties have been examined for GCPs containing poly(ethylene oxide) (PEO)/poly(ethylene glycol) (PEG) or hydrophobic alkyl groups. These systems have attracted the most attention owing to their outstanding association ability as a result of H-bonding interactions due to alkoxy groups and hydrophobic interactions[14–16] due to alkyl side chains. Nonetheless, the effects of side chains on the effective charges or ionization properties of GCPs are still unclear. In the case of GCPs grafted with hydrophilic alkoxy groups, three distinct viewpoints have been proposed. Firstly, Garrett *et al.*[17] pointed

*College of Chemistry, Beijing Normal University, Beijing 100875, China. E-mail: zhaoks@bnu.edu.cn; Tel: +86-010-58805856*

out that the effective charges on poly(methacrylic acid) (PMA) decrease as a result of proton binding due to hydrogen bonding interactions. However, Benmansour *et al.* drew an opposite conclusion,[18] by which the acidic strength of poly(4-vinylpyridinium) increases owing to steric hindrance from PEO side chains. Besides, Weber *et al.*[19] demonstrated that PEG side chains have no influence on the acidity in solution of poly-[(methyl vinyl ether)-*alt*-(maleic anhydride)]. In the case of GCPs grafted with hydrophobic alkyl groups, the effects of side chains on effective charges or ionization properties are also in dispute. Chandrasekar and Baskar[20] pointed out that the resistance to dissociation of poly(acrylamido-2-methyl-1-propanesulfonic acid) with octadecyl side chains (PAMPS-*g*-octadecyl) is similar to that of PAMPS, which was attributed to their common coil structure and the resulting ionic clusters. However, these results are different from those found by Essafi *et al.*, in which an enhancement in counterion binding due to hydrophobic side chains was indicated.[21] In addition, as far as we know, few studies have compared the joint effects of various interactions induced by side chains that provide self-association properties. Therefore, whether or not differences exist between H-bonding and hydrophobic interactions induced by side chains in controlling effective charges and structures and properties in solution is a question worth further investigation.

On the other hand, in order to better understand the temporal and spatial scales of counterion–polyelectrolyte correlations, the distribution and fluctuation of counterions have always been the focus of numerous fundamental studies.[22–24] These have included the determination of the self-diffusion coefficient, dynamic structure factor and neutralization degree of counterions *via* neutron spin echo spectroscopy (NSE), electron paramagnetic resonance (EPR), and dielectric relaxation spectroscopy (DRS), *etc.* Experimental methods for determining counterion distribution are relatively limited. The effects of hydrophobic/hydrophilic side chains on the distribution and fluctuation of counterions around PE chains have also rarely been reported.

Alternatively, dielectric relaxation spectroscopy (DRS), owing to its sensitivity to all kinds of polarization, has been used to provide micro-scale information on counterion fluctuations,[24] chain conformations,[25] concentration regimes[26] or solute hydration[27] in PE systems. The analysis of experimental DRS is based on appropriate dielectric theories and models. Earlier, Van Der Touw and Mandel[28] assumed flexible chains to be a sequence of charged rod-like subunits and derived an empirical relation between the dielectric increment and concentration. Considering the exchange of counterions between the bulk and the electric double layer, Ito and Hayakawa[29] proposed a more advanced theory based on a cell model. In this theory, scaling relations between the relaxation time and increment and the concentration were predicted, which has been supported by many simple PE solution systems.[24,26] However, deviations were still present in many complex PE solutions, for instance, those in which counterion condensation, chain entanglement or gelation occurred.[30,31] Valuable insights into counterion atmospheres and electrostatic energy on chains were not included in this theory. In recent years, Lu[32] developed a more refined double-layer polarization (DLP) model of flexible PEs, in which the counterion atmosphere was divided into an electric double layer and a bulk layer. The contributions of the structural and electrokinetic properties of PEs to relaxation were considered, and then a formula of the dielectric function in terms of the storage and loss of free energy was derived. It was confirmed that the dielectric parameters calculated using this theory were consistent with previous experimental results.[33,34]

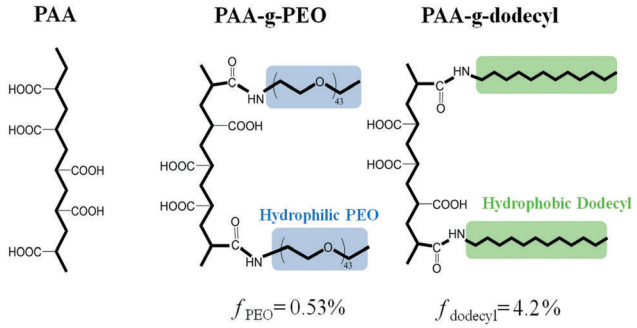


Scheme 1 Illustration of the structures of PAA, PAA-*g*-PEO and PAA-*g*-dodecyl molecules. PEO and dodecyl side chains in their respective molar fractions ($f_{PEO}$ and $f_{dodecyl}$) are randomly distributed on the PAA main chain.

To investigate and solve the abovementioned problems, in the present work we carried out dielectric measurements on poly(acrylic acid) (PAA), poly(acrylic acid)-*graft*-dodecyl (PAA-*g*-dodecyl), poly(acrylic acid)-*graft*-poly(ethylene oxide) (PAA-*g*-PEO) (Scheme 1). Dielectric spectroscopy has previously been used by our research groups on these polymers to study the effect of side chains on chain flexibility.[12] However, in that study the nature of the polyelectrolyte was not considered. In addition, the effects of side chains on the distribution and fluctuation of counterions have still not been studied. In the present study, a refined double-layer polarization (DLP) model was proposed to explain our experimental permittivity data, and valuable information about conformations and interfacial electrokinetic properties was obtained. On the basis of conductivity data, we discussed the effect of side chains on effective charges over a wide concentration range. New physical insights into the effects of electrostatic, H-bonding and hydrophobic interactions on chain conformation and the distribution and fluctuation of counterions in GCPs were obtained in detail.

## 2. Model and theory

According to the classical DLP model of rigid chains developed by Fixman,[35] each chain was simplified as a charged cylindrical tube, and the counterion atmosphere around each charged cylindrical tube was divided into an inner zone, namely, the so-called electric double layer (EDL), and an outer region, with a diameter of the order of the distance between the chains. Electrical repulsion between charged monomers was mainly shielded by the inner zone in a degressive mode. Under an ac electric field, a perturbation of the ion atmosphere was induced in the form of slow diffusion along PE chains and fast diffusion

 

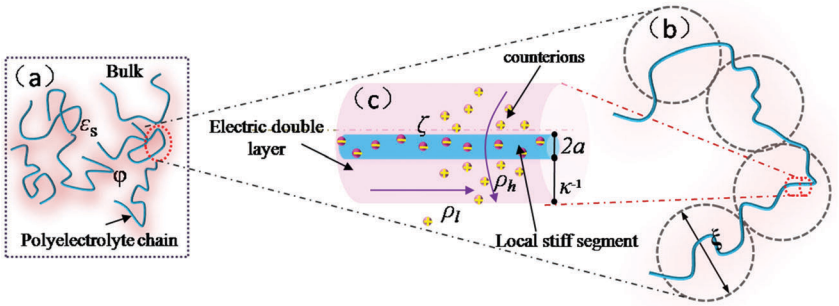


Fig. 1 Schematic of double-layer polarization (DLP) model of flexible PEs. (a) PEs with an occupied volume fraction of $\varphi$ are dispersed in a solvent with a relative dielectric constant of $\varepsilon_s$. (b) Chain configuration after a random walk of correlation blobs with a volume of $\xi^3$. (c) Local stiff segment with a radius of $a$ and an electric double layer (EDL) with a thickness of $\kappa^{-1}$, where $\zeta$ is the surface potential of the local stiff segment and $\rho_l$ and $\rho_h$ are the linear densities of counterions fluctuating along and perpendicular to the chain axis, respectively.

perpendicular to PE chains, respectively. Lu *et al.*[29] extended the abovementioned DLP model to flexible PEs by an approximation based on local stiff segments. This enables the quantification of the distribution of counterions and electrostatic repulsive energy between monomers. Moreover, coupling between the conformation and the counterion fluctuation was considered. Fig. 1 illustrates the double-layer polarization (DLP) model of flexible PEs.

PE chains with a volume fraction of $\varphi$ are dispersed in a continuous medium with a relative permittivity of $\varepsilon_s$ (Fig. 1a). The concept of a correlation blob with a diameter of $\xi$ (termed the correlation length) is introduced to describe the chain conformation. Electrostatic and hydrodynamic interactions stretch a chain within the range of the correlation length, and PE chains adopt a random walk configuration of correlation blobs (Fig. 1b). Within a correlation blob, the PE chain is composed of several stiff subunits, which are assumed to be charged cylinders with a radius of $a$ (Fig. 1c). Some counterions are closely associated with the surface of the cylinder, while the remainder are present in the electric double layer (EDL) with a thickness of $\kappa^{-1}$ (also termed the Debye length) or the bulk. On the cylinder surface $r \to a$ and the electrical potential $\Psi_0 = \zeta$, whereas far away from the cylinder $r \to \infty$ and the electrical potential $\Psi = 0$. When an ac electric current flows through the bulk and the double layer in series, the majority of the counterions in the double layer with a charge density of $\rho_h$ are made to diffuse perpendicular to the PE chains and cause high-frequency (HF) relaxation. Other counterions with a charge density of $\rho_l$ mainly diffuse along the chains and cause low-frequency relaxation.

On the basis of the DLP model described above, the complex permittivity $\varepsilon^*(\omega)$, which characterizes the dielectric property of PEs, can be derived from the contributions of counterion fluctuations along chain axes $\varepsilon_l^*(\omega)$ and perpendicular to chain axes $\varepsilon_h^*(\omega)$, respectively:

$$\varepsilon^*(\omega) = \varepsilon_l^*(\omega) + \varepsilon_h^*(\omega) + A\omega^{-m} + B\omega^{-n} \quad (1)$$

where $\omega$ (=$2\pi f$, where $f$ is the measured frequency) is the angular frequency, $A\omega^{-m}$ is the electrode polarization (EP) term of the permittivity data and the corresponding term $B\omega^{-n}$ is the electrode polarization (EP) term of the dielectric loss data. $A$, $B$, $m$, and $n$ are adjustable parameters.

The contribution of low-frequency (LF) relaxation caused by counterion fluctuations along chain axes can be expressed as:

$$\varepsilon_l^*(\omega) = \frac{\Delta\varepsilon_l}{1 + (-i\omega\xi^2/D_i)^\alpha} \quad (2)$$

where $\xi$ is the correlation length, $D_i$ ($\equiv k_B T M_i$) is the diffusivity of the counterions, $M_i$ is the mobility of the counterions, $k_B T$ is the thermal energy, and $\alpha$ is the distribution coefficient of low-frequency relaxation. The dielectric increment can be defined as:

$$\Delta\varepsilon_l = \frac{16\pi\varepsilon_s\varphi\xi}{9\ \nu\kappa^2}\left(\frac{G_l}{G_0}\right)^2 \quad (3)$$

where the volume fraction of PE chains is defined as $\varphi = N_{AV}\nu c/M_{mon}$ ($N_{AV}$ is the Avogadro constant, $\nu$ is the monomer volume, $M_{mon}$ is the molar weight of the monomer, and $c$ is the polymer concentration), $G_0$ (=$M_i q^2/l_B$) is the linear conductance of the counterions in the bulk, and $l_B$ (=$e^2/4\pi\varepsilon_s k_B T$) is the distance at which the electrostatic interaction between two elementary charges in the medium is equal to the thermal energy $k_B T$, which is also known as the Bjerrum length and is equal to 0.714 nm in this work. The contribution of counterion fluctuations along chain axes to the linear conductance can be given as:

$$G_l = M_i q \rho_l \quad (4)$$

where the linear density of counterions that cause LF relaxation can be expressed as:

$$\rho_l = -2\pi\varepsilon_0\varepsilon_s\frac{\kappa a K_1(\kappa a)}{K_0(\kappa a)}\zeta \quad (5)$$

where $\varepsilon_0$ is the dielectric constant of a vacuum and the modified Bessel function $K_\alpha(x)$ ($\alpha$ = 0, 1) is used to describe the distribution of electrical potential around the charged cylinder. In cylindrical symmetry, $K_\alpha(x)$ has the solution $\Psi = \zeta K_0(\kappa r)/K_0(\kappa a)$.

The contribution of high-frequency (HF) relaxation caused by counterion fluctuations perpendicular to chains can be expressed as:

$$\varepsilon_h^*(\omega) = \frac{\Delta\varepsilon_h}{1 + \left(\frac{-i\omega}{\omega_h}\right)^{\beta}} \quad (6)$$

where $\omega_h$ is the angular frequency of relaxation and $\beta$ is the distribution coefficient of high-frequency relaxation. The dielectric increment can be defined as:

$$\Delta\varepsilon_h = \frac{2}{9\pi^2}\frac{\varphi G_h^2 \kappa}{\omega_h^2 \varepsilon_0^2 \varepsilon_S \nu} \quad (7)$$

The contribution of counterion fluctuations perpendicular to chain axes to the linear conductance can be given as:

$$G_h = 2qM_i\rho_h\left(1 - \frac{1}{2\pi\eta l_B M_i}\right) \quad (8)$$

where $\eta$ is the viscosity of the solvent, and the linear charge density of counterions that cause HF relaxation can be given as:

$$\rho_h = \frac{\pi\varepsilon_0\varepsilon_s\zeta^2}{4k_BT}\left(\frac{\kappa a K_1(\kappa a)}{K_0(\kappa a)}\right)^2 - \frac{\pi\varepsilon_0\varepsilon_s\zeta^2(\kappa a)^2}{4k_BT} \quad (9)$$

# 3. Experiment and method

## 3.1 Materials and preparation

**3.1.1 Materials.** An aqueous solution of poly(acrylic acid) (PAA) (weight fraction of 35%, $M_w = 2.5 \times 10^5$) and potassium bis(trimethylsilyl)amide (0.5 mol $L^{-1}$ solution in toluene) were purchased from Sigma-Aldrich, and 2-chloro-4,6-dimethoxy-1,3,5-triazine (CDMT) was purchased from Beijing F&F Chemical Co., Ltd. *N*-Methylmorpholine (NMM), *N*-(3-dimethylaminopropyl)-*N*-ethylcarbodiimide hydrochloride (EDC) and 1-hydroxybenzotriazole (HOBt) were purchased from Shanghai Medpep Co., Ltd. Ethyl ether, acetic acid, sodium hydroxide and tetrahydrofuran (THF) were purchased from Beijing Chemical Works. Dodecylamine was purchased from Sinopharm Chemical Reagent Co., Ltd and was used without further purification. *N*,*N*-Dimethylformamide (DMF) was also provided by Beijing Chemical Works. The water used in this study was purified by distillation with a Rios water system (Millipore Corp., USA). A dialysis bag was purchased from Beijing Jingkehongda Biotechnology Co., Ltd and was pretreated by a process comprising successive boiling in a mixed solution of 1 : 1 ethanol/water, 0.001 M 2-[2-(bis(carboxymethyl)-amino)ethyl(carboxymethyl)amino]acetic acid (EDTA) and 0.01 M $NaHCO_3$.

**3.1.2 Preparation of samples.** Solid samples of PAA-*g*-PEO and PAA-*g*-dodecyl (Scheme 1) were prepared and purified by the research group of Prof. Charles C. Han at the Chinese Academy of Sciences (Beijing, P. R. China) according to a previously described method.[16] Firstly, amine-terminated PEO was synthesized by the route reported by Yokoyama *et al.*[36] Secondly, using EDC and HOBt, PAA-*g*-PEO was synthesized by the classical reaction of amino groups with carboxylic groups, and by using DMTMM (4-(4,6-dimethoxy-1,3,5-triazin-2-yl)-4-methylmorpholinium chloride), PAA-*g*-dodecyl was also synthesized. The crude product of PAA-*g*-PEO that was obtained was dialyzed against water for 4 days. The crude product of PAA-*g*-dodecyl was dialyzed against an acidic mixed solution of water and ethanol and then pure water. Finally, pure solid samples of PAA, PAA-*g*-PEO and PAA-*g*-dodecyl were obtained by freeze-drying. Detailed structural parameters of PAA, PAA-*g*-PEO and PAA-*g*-dodecyl are listed in Table 1. The compositions and molecular weights of these copolymers were determined by $^1$H NMR measurements. A solid sample of PAA-*g*-PEO was dissolved in a water/THF solvent and then dodecylamine was added. PAA-*g*-PEO-*g*-dodecyl was prepared by adding DMTMM. Finally, pure solid PAA-*g*-PEO-*g*-dodecyl was obtained by a process comprising rotary evaporation, dialysis and freeze-drying.

Table 1 Molecular characteristics of PAA, PAA-*g*-PEO, and PAA-*g*-dodecyl, including their molecular weight ($M_w$), molar fraction of PEO or dodecyl groups ($f_{PEO}$, $f_{dodecyl}$), and weight fraction of PEO or dodecyl groups ($w_{PEO}$, $w_{dodecyl}$)

| | $M_w/10^5$ | $w_{PEO}$ (wt%) | $w_{dodecyl}$ (wt%) | $f_{PEO}$ (mol%) | $f_{dodecyl}$ (mol%) |
|---|---|---|---|---|---|
| PAA | 2.5 | — | — | — | — |
| PAA-*g*-PEO | 2.9 | 13 | — | 0.53 | — |
| PAA-*g*-dodecyl | 2.8 | 10 | — | — | 4.2 |

Solid samples of PAA, PAA-*g*-PEO and PAA-*g*-dodecyl (120 mg) were initially dissolved in 250 μL DMF and 6 mL double-distilled water (specific resistance of higher than 16 MΩ cm). The pH of these initial solutions was adjusted to around 7.5 by slowly dripping very small amounts of KOH (0.5 mol $L^{-1}$) using a microprocessor pH meter.

A series of aqueous solutions of PAA (0.025–19.5 mg $mL^{-1}$), PAA-*g*-PEO (0.025–19.5 mg $mL^{-1}$) and PAA-*g*-dodecyl (0.025–2.5 mg $mL^{-1}$) were prepared by adding a given volume of double-distilled water to these initial solutions.

## 3.2 Dielectric measurements

Dielectric measurements of aqueous solutions of PAA, PAA-*g*-PEO and PAA-*g*-dodecyl over the measured concentration range were carried out using a 4294A precision impedance analyzer (Agilent Technologies) from 40 Hz to 110 MHz. The applied alternating field was 500 mV, and a measurement cell with concentric cylindrical platinum electrodes was employed (the effective area of the electrodes was 78.5 $mm^2$, and the diameters of the inner and outer cylindrical electrodes were 5 mm and 10 mm, respectively). All measurements were carried out at room temperature (30 ± 0.5 °C). Firstly, the measured raw data for capacitance $C_x$ and conductance $G_x$ were corrected to eliminate errors from residual inductance ($L_r$) and stray capacitance ($C_r$) according to the Schwan method.[37] Then, the corrected values of the capacitance $C_s$ and conductance $G_s$ were converted to the corresponding dielectric permittivity $\varepsilon$ and conductivity $\kappa$ using the equations $\varepsilon' = C_s/C_1$ and $\kappa = G_s\varepsilon_0/C_1$.

### 3.3 Determination of structural and electrical parameters

Under an applied ac electric field, the complex permittivity $\varepsilon^*(\omega)$ can be expressed as:

$$\varepsilon^*(\omega) = \varepsilon(\omega) - j\varepsilon''(\omega) \quad (10)$$

where $\varepsilon(\omega)$ is the real part of the complex permittivity (also termed the permittivity), $j = (-1)^{1/2}$, and $\varepsilon''(\omega)$ is the dielectric loss, which was determined by subtracting the low-frequency limit of the conductivity $\sigma_l$ (termed the dc conductivity) from the total conductivity $\sigma(\omega)$ using the following equation:

$$\varepsilon''(\omega) = \frac{(\sigma(\omega) - \sigma_l)}{\omega\varepsilon_0} \quad (11)$$

By combining eqn (1)–(9) in Section 2, the calculated permittivity spectrum for the DLP model was determined by fixing the variable parameters $\xi$, $\kappa^{-1}$, $\rho_l$, and $\rho_h$. In our work, the experimental permittivity spectra with the electrode polarization (EP) effect for PAA, PAA-*g*-PEO and PAA-*g*-dodecyl were fitted to the theoretical permittivity spectrum over the measured concentration range. The best curve fitting was guaranteed by using the non-linear least-squares method. Once fitting was performed well, the EP term $A\omega^{-m}$ was obtained. Then, a new permittivity spectrum without the EP effect was derived by subtracting the EP term. Moreover, many valuable structural ($\kappa^{-1}$ and $\xi$) and electrical parameters ($\rho_l$ and $\rho_h$) were determined for the three samples. Then, the LF and HF relaxation increments were calculated by substituting $\rho_l$, $\rho_h$, $\kappa^{-1}$ and $\xi$ into eqn (3), (4), (7) and (8), respectively. Finally, the zeta electrical potential $\zeta$ on the surface of the local stiff segments was calculated by substituting the parameters $\rho_l$, $\rho_h$ and $\kappa^{-1}$ into eqn (5) and (9).

# 4. Results and discussion

### 4.1 Effect of side chains on the evolution of chain conformation

**4.1.1 Dielectric spectra and dielectric analysis with DLP model.** Fig. 2 shows three-dimensional representations of the dielectric loss spectra of aqueous solutions of PAA (a), PAA-*g*-PEO (b) and PAA-*g*-dodecyl (c) over the entire concentration range. In Fig. 2, two sub-relaxation processes can be seen for all three systems over relatively LF and HF ranges (red arrows). Then, the experimental permittivity spectra were fitted to the theoretical permittivity spectra calculated by the double-layer polarization (DLP) model, as described in Section 2. Representative fitting results for three samples with concentrations of 0.05 mg mL$^{-1}$ are shown in Fig. 3(a–c) It can be seen that all three experimental permittivity spectra (hollow circles) are highly consistent with the corresponding calculated permittivity spectra (lines). In other words, the DLP model exhibited excellent performance in predicting the dielectric properties of the three samples. According to the DLP theory,[32] it is easy to assign the LF and HF dielectric relaxation to the fluctuation of counterions along the entire chain axes and perpendicular to the chain axes, respectively. On the basis of dielectric analysis by the method described in Section 3.3, several valuable structural and electrical parameters of the three samples at varying concentrations were determined, and the results are listed in Table 2.

Then, the dielectric loss spectra and permittivity spectra of these samples were compared. In Fig. 2, some differences are clearly observed despite their shape and trend of concentration dependence between the dielectric loss spectra of aqueous solutions of PAA-*g*-PEO (b), PAA-*g*-dodecyl (c) and PAA (a). In addition, we can seen in Fig. 3 that the LF and HF dielectric increments for PAA-*g*-PEO were both larger than those for PAA,

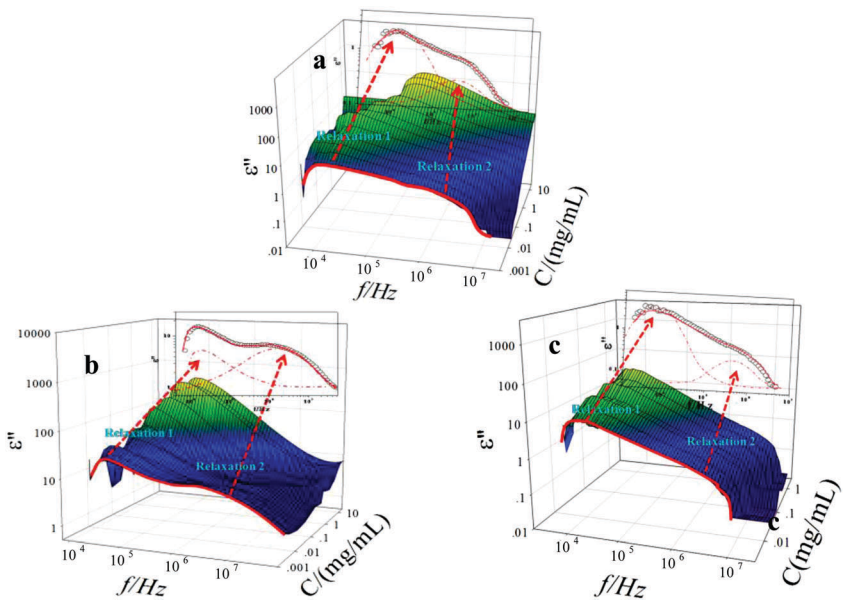


Fig. 2 Three-dimensional representations of dielectric loss spectra of aqueous solutions of PAA (a), PAA-*g*-PEO (b), and PAA-*g*-dodecyl (c) at a series of concentrations after eliminating the effect of electrode polarization.

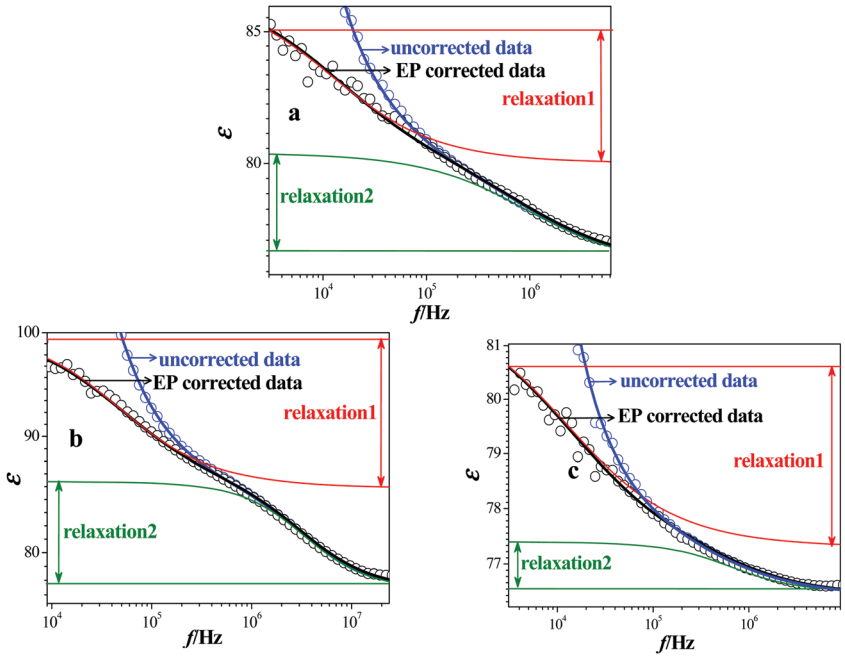


Fig. 3 Representative results of fitting the permittivity spectra of solutions of PAA (a), PAA-*g*-PEO (b), and PAA-*g*-dodecyl (c) with concentrations of 0.05 mg mL$^{-1}$ using the following parameters: Bjerrum length $l_B$ = 0.714 nm, solvent viscosity $\eta$ = 0.837 × 10$^{-3}$ N s m$^{-2}$ measured by a viscosimeter at 30 °C, dielectric constant of a vacuum $\varepsilon_0$ = 8.854187817 × 10$^{-12}$ F m$^{-1}$, relative dielectric constant of the solvent $\varepsilon_s$ = 76. The hollow circles represent experimental permittivity data and the solid lines represent theoretical permittivity data calculated by the DLP model of flexible PEs. The blue and black circles (lines) represent permittivity data before and after subtraction of the EP effect, respectively. The LF and HF relaxation increments are represented by red and green lines (arrows).

and those for PAA-*g*-dodecyl were smaller than those for PAA (red and green arrows). This strongly indicates that the number or fluctuation distance of counterions for PAA-*g*-PEO was larger than those for PAA, whereas the reverse was true for PAA-*g*-dodecyl, which cannot exclude possible changes in chain conformation or effective charge on PAA due to the presence of PEO or dodecyl side chains.[24] Determining exactly how side chains affect the chain conformation and electrical properties of PAA is the purpose of our study and will be discussed in detail in the following sections.

**4.1.2 Chain aggregation in different concentration regimes.** Fig. 4a and b show plots of dielectric parameters as functions of concentration for aqueous solutions of PAA, PAA-*g*-PEO, and PAA-*g*-dodecyl. Clearly, there are two transitional regions, which divide the solution concentration range into three concentration regimes, for PAA and PAA-*g*-PEO and one transitional region, which divides the solution concentration range into two concentration regimes, for PAA-*g*-dodecyl. In general, PE solutions are characterized by a transition from a dilute non-entanglement regime *via* a semi-dilute non-entanglement regime to a semi-dilute entanglement regime.[3,38] Within the dilute concentration regime, polymer coils are isolated from each other and the solution properties are independent of various inter-chain interactions. When the solution concentration is close to the crossover concentration $c^*$, polymer chains begin to overlap, and at this point the volume fraction of PE chains is 1. In theory, the crossover concentration $c^*$ can be expressed as a function of the radius of gyration $R_g$ and scales with the effective fraction of monomers $f_i$ on chains:[3,39]

$$c^* = \frac{N}{R_g^3 N_A} \sim f_i^{\theta} \quad (12)$$

where $N$ is the number of monomers per chain and $N_A$ is the Avogadro constant. The value of the coefficient $\theta$ is −2 for PEs in good solvents and −3 for polymers in poor solvents. According to the work reported by Li *et al.*, the crossover concentration $c^*$ of PAA-*g*-PEO ($w_{PEO}$ = 10%, $M_w$ = 2.87 × 10$^5$) was estimated to be around 0.2 mg mL$^{-1}$, which was close to the first transitional region around 0.15 mg mL$^{-1}$ in our work, as shown in Fig. 4. In addition, the results of a light scattering experiment by Hao *et al.* showed that at concentrations of less than approximately 0.3 mg mL$^{-1}$, PAA-*g*-dodecyl existed in the form of isolated chains, whereas at higher concentrations PAA-*g*-dodecyl molecules overlapped and were entangled with each other. Therefore, it is not difficult to conclude that the transitional concentrations of aqueous solutions of PAA, PAA-*g*-PEO, and PAA-*g*-dodecyl of less than 1 mg mL$^{-1}$ shown in Fig. 4 represent crossover concentrations. Furthermore, by substituting the crossover concentration $c^*$ of PAA (on the left in Fig. 4) into eqn (12), the radius of gyration $R_g$ of PAA in the region of $c^*$ (∼0.5 mg mL$^{-1}$) was calculated to be 22.6 nm. Reith *et al.* measured $R_g$ values of PAA at various solution concentrations and molecular weights $M_w$. The results showed that the radius of gyration $R_g$ of PAA with a molecular weight of ∼2.04 × 10$^5$ and a solution concentration of ∼0.5 mg mL$^{-1}$

 

Table 2 Structural and electrical parameters of PAA, PAA-*g*-PEO, and PAA-*g*-dodecyl in solutions of different concentrations determined by dielectric analysis as described in Section 3.3

| $c$ (mg mL$^{-1}$) | $\rho_l \times 10^{20}$ (C nm$^{-1}$) | $\rho_h \times 10^{19}$ (C nm$^{-1}$) | $\xi$ (nm) | $\kappa^1$ (m) | $\zeta$ (mV) | $\Delta\varepsilon_l$ | $\Delta\varepsilon_h$ | $\tau_l$ (μs) | $\tau_h$ (ns) | $\sigma_l$ (mS m$^{-1}$) |
|---|---|---|---|---|---|---|---|---|---|---|
| PAA | | | | | | | | | | |
| 0.0125 | 0.682 ± 0.020 | 2.20 ± 0.090 | 49.2 ± 0.32 | 38.1 ± 0.29 | 48.3 ± 0.34 | 2.87 ± 0.080 | 1.10 ± 0.11 | 37.0 ± 0.23 | 315 ± 6.3 | 0.814 ± 0.026 |
| 0.025 | 0.682 ± 0.020 | 2.10 ± 0.12 | 48.0 ± 0.35 | 35.4 ± 0.28 | 45.58 ± 0.34 | 5.09 ± 0.090 | 1.61 ± 0.12 | 35.1 ± 0.24 | 274 ± 5.1 | 1.20 ± 0.020 |
| 0.05 | 0.686 ± 0.020 | 2.35 ± 0.070 | 43.5 ± 0.31 | 28.9 ± 0.27 | 38.2 ± 0.31 | 6.22 ± 0.080 | 2.22 ± 0.15 | 34.5 ± 0.26 | 212 ± 5.3 | 1.80 ± 0.024 |
| 0.1 | 0.668 ± 0.020 | 2.40 ± 0.090 | 39.0 ± 0.29 | 25.8 ± 0.25 | 33.3 ± 0.30 | 8.67 ± 0.080 | 3.14 ± 0.13 | 30.0 ± 0.27 | 159 ± 4.4 | 3.00 ± 0.041 |
| 0.25 | 0.637 ± 0.030 | 2.65 ± 0.13 | 34.5 ± 0.31 | 22.4 ± 0.24 | 27.5 ± 0.32 | 13.1 ± 0.090 | 3.97 ± 0.15 | 25.0 ± 0.21 | 110 ± 4.8 | 6.00 ± 0.053 |
| 0.5 | 0.678 ± 0.020 | 4.25 ± 0.16 | 25.5 ± 0.25 | 20.0 ± 0.21 | 26.6 ± 0.29 | 17.1 ± 0.10 | 5.12 ± 0.17 | 20.0 ± 0.19 | 80.0 ± 4.5 | 9.00 ± 0.061 |
| 1 | 0.731 ± 0.030 | 5.75 ± 0.13 | 18.2 ± 0.34 | 16.2 ± 0.27 | 22.9 ± 0.22 | 18.7 ± 0.08 | 6.57 ± 0.2 | 13.3 ± 0.19 | 55.8 ± 3.5 | 17.4 ± 0.096 |
| 2 | 0.874 ± 0.040 | 6.65 ± 0.20 | 12.9 ± 0.20 | 12.9 ± 0.21 | 20.9 ± 0.25 | 22.1 ± 0.14 | 8.00 ± 0.22 | 8.69 ± 0.15 | 43.0 ± 3.4 | 26.6 ± 0.096 |
| 4 | 0.963 ± 0.030 | 7.50 ± 0.17 | 9.30 ± 0.17 | 10.9 ± 0.18 | 19.3 ± 0.26 | 27.1 ± 0.14 | 9.31 ± 0.24 | 6.06 ± 0.080 | 34.6 ± 3.5 | 48.0 ± 0.11 |
| 6 | 0.989 ± 0.040 | 7.75 ± 0.14 | 7.70 ± 0.24 | 9.95 ± 0.19 | 18.2 ± 0.28 | 29.8 ± 0.16 | 11.7 ± 0.22 | 4.00 ± 0.060 | 28.7 ± 2.3 | 67.0 ± 0.16 |
| 10 | 1.18 ± 0.070 | 8.00 ± 0.13 | 6.30 ± 0.18 | 8.94 ± 0.19 | 18.3 ± 0.30 | 37.4 ± 0.15 | 14.1 ± 0.28 | 3.00 ± 0.070 | 25.7 ± 2.2 | 110 ± 0.24 |
| 13 | 1.25 ± 0.090 | 9.65 ± 0.15 | 5.35 ± 0.23 | 8.30 ± 0.18 | 20.0 ± 0.34 | 56.7 ± 0.31 | 13.6 ± 0.29 | 2.78 ± 0.070 | 21.8 ± 2.2 | 141 ± 0.37 |
| 19.5 | 1.39 ± 0.090 | 9.90 ± 0.22 | 4.43 ± 0.19 | 7.90 ± 0.17 | 21.2 ± 0.36 | 75.9 ± 0.38 | 11.4 ± 0.22 | 2.53 ± 0.080 | 21.1 ± 2.4 | 190 ± 0.54 |
| PAA-*g*-PEO | | | | | | | | | | |
| 0.0125 | 0.980 ± 0.032 | 5.25 ± 0.15 | 62.0 ± 0.57 | 47.0 ± 0.36 | 89.2 ± 0.79 | 10.6 ± 0.25 | 17.8 ± 0.21 | 15.4 ± 0.29 | 159 ± 4.0 | 3.00 ± 0.056 |
| 0.025 | 0.816 ± 0.020 | 5.10 ± 0.15 | 59.0 ± 0.55 | 44.7 ± 0.35 | 70.5 ± 0.72 | 12.4 ± 0.26 | 14.2 ± 0.21 | 15.4 ± 0.28 | 116 ± 3.0 | 3.58 ± 0.059 |
| 0.05 | 0.849 ± 0.020 | 5.40 ± 0.15 | 56.5 ± 0.55 | 37.8 ± 0.32 | 59.6 ± 0.64 | 14.9 ± 0.26 | 9.98 ± 0.20 | 15.4 ± 0.28 | 72.3 ± 2.0 | 5.00 ± 0.062 |
| 0.1 | 0.891 ± 0.020 | 5.57 ± 0.17 | 51.2 ± 0.53 | 28.9 ± 0.29 | 49.6 ± 0.58 | 20.6 ± 0.31 | 8.99 ± 0.20 | 15.2 ± 0.29 | 45.5 ± 2.0 | 7.00 ± 0.076 |
| 0.25 | 0.981 ± 0.030 | 7.60 ± 0.18 | 39.3 ± 0.46 | 21.3 ± 0.27 | 38.3 ± 0.52 | 24.6 ± 0.34 | 10.1 ± 0.20 | 12.6 ± 0.24 | 33.5 ± 2.0 | 11.0 ± 0.11 |
| 0.5 | 0.939 ± 0.030 | 8.00 ± 0.18 | 29.5 ± 0.42 | 17.6 ± 0.26 | 32.0 ± 0.52 | 25.9 ± 0.34 | 10.0 ± 0.24 | 12.1 ± 0.24 | 31.8 ± 2.0 | 17.3 ± 0.14 |
| 1 | 0.939 ± 0.030 | 8.50 ± 0.18 | 22.5 ± 0.37 | 14.9 ± 0.24 | 27.0 ± 0.48 | 27.6 ± 0.34 | 11.4 ± 0.24 | 10.0 ± 0.20 | 25.3 ± 1.0 | 28.0 ± 0.21 |
| 2 | 1.02 ± 0.040 | 8.75 ± 0.17 | 15.5 ± 0.35 | 12.4 ± 0.24 | 24.4 ± 0.47 | 32.8 ± 0.35 | 11.7 ± 0.24 | 7.25 ± 0.16 | 22.1 ± 1.0 | 43.0 ± 0.32 |
| 4 | 1.02 ± 0.040 | 9.00 ± 0.20 | 11.0 ± 0.35 | 10.8 ± 0.22 | 21.4 ± 0.42 | 36.1 ± 0.37 | 11.5 ± 0.26 | 5.03 ± 0.13 | 18.7 ± 0.56 | 66.0 ± 0.35 |
| 6 | 1.18 ± 0.050 | 9.80 ± 0.21 | 9.00 ± 0.34 | 9.12 ± 0.22 | 20.9 ± 0.42 | 42.6 ± 0.38 | 13.5 ± 0.29 | 3.57 ± 0.11 | 15.9 ± 0.57 | 95.0 ± 0.45 |
| 10 | 1.22 ± 0.050 | 10.5 ± 0.22 | 7.20 ± 0.35 | 8.45 ± 0.22 | 22.5 ± 0.42 | 65.5 ± 0.43 | 13.6 ± 0.29 | 3.45 ± 0.11 | 16.8 ± 0.57 | 117 ± 0.63 |
| 13 | 1.31 ± 0.040 | 10.8 ± 0.22 | 6.02 ± 0.32 | 7.90 ± 0.22 | 24.0 ± 0.42 | 86.5 ± 0.56 | 13.0 ± 0.29 | 3.10 ± 0.11 | 15.9 ± 0.57 | 164 ± 0.63 |
| 19.5 | 1.53 ± 0.060 | 10.8 ± 0.22 | 5.80 ± 0.28 | 7.60 ± 0.23 | 26.6 ± 0.45 | 104 ± 0.93 | 15.2 ± 0.34 | 2.86 ± 0.080 | 15.9 ± 0.57 | 169 ± 0.82 |
| PAA-*g*-dodecyl | | | | | | | | | | |
| 0.025 | 0.532 ± 0.020 | 1.75 ± 0.070 | 47.0 ± 0.34 | 36.5 ± 0.29 | 38.4 ± 0.28 | 2.88 ± 0.080 | 0.739 ± 0.080 | 37.0 ± 0.23 | 265 ± 5.0 | 0.95 ± 0.031 |
| 0.05 | 0.507 ± 0.020 | 1.80 ± 0.070 | 44.5 ± 0.32 | 31.6 ± 0.27 | 31.9 ± 0.25 | 3.22 ± 0.10 | 0.751 ± 0.060 | 32.2 ± 0.20 | 156 ± 5.0 | 1.40 ± 0.025 |
| 0.1 | 0.508 ± 0.020 | 1.80 ± 0.070 | 43.0 ± 0.32 | 25.8 ± 0.25 | 26.2 ± 0.23 | 4.29 ± 0.11 | 0.857 ± 0.090 | 31.2 ± 0.20 | 128 ± 3.5 | 2.10 ± 0.022 |
| 0.15 | 0.539 ± 0.020 | 2.00 ± 0.070 | 34.5 ± 0.28 | 22.4 ± 0.23 | 23.3 ± 0.23 | 4.90 ± 0.11 | 0.937 ± 0.090 | 31.2 ± 0.20 | 118 ± 3.5 | 2.58 ± 0.020 |
| 0.3 | 0.538 ± 0.020 | 2.65 ± 0.080 | 27.0 ± 0.25 | 21.3 ± 0.23 | 22.2 ± 0.23 | 6.97 ± 0.14 | 1.10 ± 0.090 | 29.4 ± 0.20 | 109 ± 3.5 | 4.30 ± 0.051 |
| 0.5 | 0.572 ± 0.020 | 2.90 ± 0.080 | 20.0 ± 0.21 | 17.1 ± 0.20 | 20.2 ± 0.22 | 7.10 ± 0.14 | 1.20 ± 0.11 | 21.7 ± 0.14 | 99.4 ± 3.5 | 4.64 ± 0.056 |
| 0.9 | 0.695 ± 0.030 | 3.00 ± 0.080 | 16.0 ± 0.19 | 14.6 ± 0.17 | 20.2 ± 0.22 | 10.6 ± 0.18 | 1.44 ± 0.10 | 12.6 ± 0.10 | 83.8 ± 3.0 | 8.50 ± 0.071 |
| 1.5 | 0.699 ± 0.030 | 3.10 ± 0.080 | 12.0 ± 0.15 | 12.5 ± 0.14 | 19.0 ± 0.21 | 10.4 ± 0.18 | 1.68 ± 0.10 | 9.09 ± 0.070 | 88.4 ± 3.0 | 11.4 ± 0.091 |
| 2.5 | 0.711 ± 0.030 | 3.40 ± 0.080 | 8.50 ± 0.11 | 9.75 ± 0.10 | 16.4 ± 0.20 | 8.57 ± 0.15 | 1.85 ± 0.10 | 3.45 ± 0.040 | 86.8 ± 3.0 | 18.1 ± 0.13 |

is 22.1 nm,[40] which is close to the abovementioned value of 22.6 nm calculated in our work for PAA with a molecular weight of $\sim 2.5 \times 10^5$ at 0.5 mg mL$^{-1}$. It is therefore further indicated that the initial transitional region corresponds to the region of the crossover concentration $c^*$. In addition, within the semi-dilute concentration regime, the width of the non-entanglement regime as represented by $c^e/c^*$ for an aqueous solution of PAA ($M_w = 2.5 \times 10^5$) has been estimated to be about 21 by light scattering and viscometry measurements,[41] which is very similar to the ratio of the second to the first transitional concentration ($c_2/c_1 \approx 22$) in our work (on the left in Fig. 4). Therefore, it can be further concluded that the second transitional region in Fig. 4 corresponds to the entanglement concentration $c^e$. The crossover concentration and entanglement concentration $c^e$ of the three samples are listed in Table 3. According to the theory of the entanglement of polymer solutions,[39] the internal movement of each chain is restricted by $n^e$ other chains at the onset of entanglement. The number of entangled chains $n^e$ is determined by the width of the non-entanglement regime to be $c^e/c^* = n^4$, which is an index that reflects the character of a polyelectrolyte chain. By substituting the crossover concentration and entanglement concentration $c^e$ into $c^e/c^*$, the number of entangled chains $n^e$ was estimated and is also listed in Table 3. It is shown that although the values of $c^*$ and $c^e$ of PAA-*g*-PEO and PAA-*g*-dodecyl are lower than that of PAA, the value of $n$ for PAA-*g*-PEO is higher than that for PAA, which indicates that the crossover capabilities of PAA-*g*-PEO and PAA-*g*-dodecyl are greater than that of PAA, and the entanglement capability of PAA-*g*-PEO is also greater than that of PAA. On the one hand, this result is predictable because the PEO and dodecyl side chains introduce hydrogen bonding and hydrophobic interactions between the chains, which make them overlap and become entangled more easily. The long PEO side chains also contribute to higher entanglement capability between chains. On the other hand, $c^*$ is proportional to the fraction of effective charges on chains $f_i$, as shown in eqn (12). Moreover, the entanglement capability also decreases owing to electrical repulsion interactions between monomers. Therefore, a further detailed investigation of the

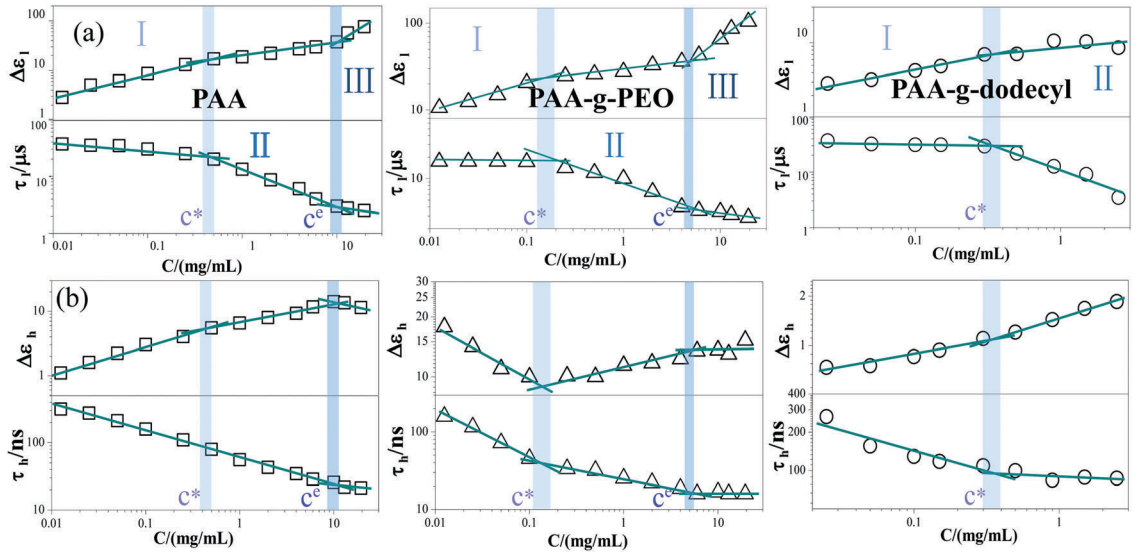


Fig. 4 Concentration dependences of dielectric increment and relaxation time of LF relaxation ($\Delta\varepsilon_l$ and $\tau_l$) (a) and HF relaxation ($\Delta\varepsilon_h$ and $\tau_h$) (b) for aqueous solutions of PAA, PAA-*g*-PEO, and PAA-*g*-dodecyl. Here, I, II and III represent the dilute, semi-dilute non-entanglement and semi-dilute entanglement concentration regimes.

Table 3 Comparison of crossover concentration $c^*$, entanglement concentration $c^e$ and number of entangled chains $n^e$ for PAA, PAA-*g*-PEO and PAA-*g*-dodecyl, obtained from the dielectric parameters in Table 2

| | PAA | PAA-*g*-PEO | PAA-*g*-DA |
|---|---|---|---|
| $c^*$/(mg mL$^{-1}$) | 0.5 | 0.15 | 0.35 |
| $c^e$/(mg mL$^{-1}$) | 10 | 5.5 | — |
| $c^e/c^*$ | 20 | 33.3 | — |
| $n^e$ | 2.11 | 2.4 | — |

effects of side chains on effective charges or ionization properties will be worthwhile to better understand the conformation and aggregation of chains.

**4.1.3 Effect of side chains on the effective charges on chains.** Firstly, the effective charges (net charges) on chains were estimated from the linear density of counterions around chains ($\rho = \rho_l + \rho_h$), which was determined by the dielectric analysis method described in Section 3.3. As listed in Table 2, the linear charge densities of PAA-*g*-PEO and PAA-*g*-dodecyl at 0.025 mg mL$^{-1}$ were about 2.44 and 0.75 times that of PAA, respectively. This result strongly indicates that PEO side chains increase the number of net charges on PAA, whereas dodecyl side chains decrease it. In order to examine the concentration dependence of the effect of side chains on $f_i$, we then examined dc conductivity data for aqueous solutions of PAA, PAA-*g*-PEO, PAA-*g*-dodecyl and PAA-*g*-PEO-*g*-dodecyl ($M_w = 3.1 \times 10^5$, $w_{PEO} = 10\%$, $w_{dodecyl} = 13\%$, $f_{PEO} = 0.5\%$, $f_{dodecyl} = 4.2\%$) of varying concentrations. From a phenomenological point of view, the conductivity of a PE solution in response to an external applied electric field depends on the numerical concentration, valence and mobility of charged entities. Here, the contribution of PE chains to conductivity can be ignored because their mobility is extremely low in comparison to that of counterions. The conductivity of a PE solution thus approximately follows this relationship:[24]

$$\sigma = Ze n_i \mu \tag{13}$$

Here i refers to counterions, $Z_i$ is the valence of the counterions, $n_i$ is the numerical concentration of the counterions ($n_i = f_i N n$, where $f_i$ is the fraction of effective charges without additional salts and $n$ is the numerical concentration of the charged polymer), and $\mu$ is the mobility of the counterions, which is related to the temperature $T$ and diffusion coefficient $D$:

$$\mu = \frac{D}{RT} \tag{14}$$

in which the diffusion coefficient $D$ is defined by the Stokes–Einstein equation:

$$D = \frac{k_B T}{6\pi\eta r_0} \tag{15}$$

where $r_0$ is the radius of the counterions and $\eta$ is the viscosity of the solvent. By combining eqn (13)–(15), the conductivity can be redefined as:

$$\sigma = \frac{k_B Z_i f_i e N n_P}{6\pi\eta r_0} \tag{16}$$

According to eqn (16), the ratios of the fractions of effective charges on PAA-*g*-PEO, PAA-*g*-dodecyl and PAA-*g*-PEO-*g*-dodecyl to that on PAA ($f_i/f_{i\text{-PAA}}$) can be estimated from the ratios of the measured LF conductivities ($\sigma_i/\sigma_{i\text{-PAA}}$) of PAA, PAA-*g*-PEO, PAA-*g*-dodecyl and PAA-*g*-PEO-*g*-dodecyl. The results are presented in Fig. 5.

From Fig. 5, the value of $f_{i\text{-PAA-}g\text{-PEO}}/f_{i\text{-PAA}}$ at 0.025 mg mL$^{-1}$ is about 2.95 and that of $f_{i\text{-PAA-}g\text{-dodecyl}}/f_{i\text{-PAA}}$ is about 0.8, which are similar to the values of 2.44 and 0.75 estimated from the results for counterion density in Table 2. In addition, it can be seen that the effective charges on PAA-*g*-PEO are obviously greater than those on PAA (red line: $f_{i\text{-PAA-}g\text{-PEO}}/f_{i\text{-PAA}} > 1$), whereas the reverse is true for PAA-*g*-dodecyl (green line: $f_{i\text{-PAA-}g\text{-dodecyl}}/f_{i\text{-PAA}} < 1$) below around 10 mg mL$^{-1}$. This is therefore sufficient to

 

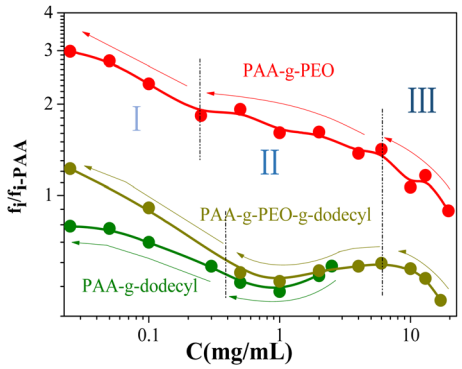


Fig. 5 Ratios of the fractions of effective charges on PAA-*g*-PEO, PAA-*g*-dodecyl and PAA-*g*-PEO-*g*-dodecyl to that on PAA ($f_i/f_{i\text{-}PAA}$) in aqueous solution as a function of the polymer concentration.

confirm the completely different roles of PEO and dodecyl side chains in changing the fraction of effective charges on PAA. In the case of PAA-*g*-PEO, two effects are generally introduced by the side chains: one is their high proton binding energy, which leads to the formation of H-bonds,[42] and the other is their steric hindrance effect, as they inevitably occupy some space near chains and thus less space is available to accommodate condensed counterions. If we assume that the former effects play a dominant role, the value of $f_{i\text{-}PAA\text{-}g\text{-}PEO}$ will be lower than that of $f_{i\text{-}PAA}$, which is not in accordance with the results for $\rho_l$ (Table 2) and the fraction of effective charges $f_i$ (Fig. 5). Another mechanism, namely, the steric hindrance effect of PEO, can be estimated in terms of the volume fraction $\Phi$ of PEO side chains around a polymer coil as follows:[18,43]

$$\varphi_{PEO} = \frac{M_{PEO}}{\frac{4\pi}{3} N_A d R_g^3} \quad (17)$$

where $d$ is the density of PEO coils ($\sim 0.8$ g mL$^{-1}$). An empirical relationship for the radius of gyration of PEO was derived by Benkhira *et al.*:[44]

$$R_g = 0.082 M_{PEO}^{0.64} \quad (18)$$

By combining eqn (17) and (18), the value of $\varphi_{PEO}$ is calculated to be 0.745. This implies that the PEO side chains occupy most of the volume near chains, so that more counterions remain free but are not condensed near chains. In contrast, counterions in the case of PAA-*g*-dodecyl more easily condense in the microdomain composed of dodecyl side chains with a low dielectric environment.[21] Therefore, the value of $f_{i\text{-}PAA\text{-}g\text{-}dodecyl}$ is lower than that of $f_{i\text{-}PAA}$ (Fig. 5).

With respect to the evolution of effective charges with concentration, we further analyzed the effect of side chains in dilute and semi-dilute solutions. In Fig. 5, as the concentration decreases in regimes II and III (identified as the semi-dilute entanglement regime), it is interesting to see a notable increase in the value of $f_{i\text{-}PAA\text{-}g\text{-}PEO}/f_{i\text{-}PAA}$, which implies that the promotion effect on ionization properties caused by PEO side chains was gradually enhanced during the dilution process. Within regimes II and III, intermolecular hydrogen bonds between carboxylic groups and ether oxygen atoms in PEO side chains are known to exist.[42] Moreover, these hydrogen bonds are easily broken in the process of solution dilution, which probably yields additional free carboxylic acid groups, which can further dissociate into $COO^-$ and $H^+$ ions, as illustrated in Fig. 7a. In addition, as mentioned above, most of these $H^+$ ions remain free owing to the steric hindrance effect of PEO side chains.[18] A direct consequence of these processes is the notable increase in the value of $f_{i\text{-}PAA\text{-}g\text{-}PEO}/f_{i\text{-}PAA}$ mentioned above. For PAA-*g*-dodecyl, as shown in Fig. 5, as the concentration decreases in regime II (identified as a semi-dilute regime), it is clearly seen that the value of $f_{i\text{-}PAA\text{-}g\text{-}dodecyl}/f_{i\text{-}PAA}$ decreases slightly, which suggests that the inhibitory effect on ionization properties caused by dodecyl side chains was slightly enhanced during the dilution process. In general, condensed counterions tend to be released as a solution is diluted.[3] As illustrated in Fig. 7c, the abovementioned slight decrease in the value of $f_{i\text{-}PAA\text{-}g\text{-}dodecyl}/f_{i\text{-}PAA}$ in regime II probably arises from the continuous condensation of counterions into the hydrophobic dodecyl microdomain, which were released during the dilution process.

Fig. 6 shows plots of the ζ-potential results for PAA, PAA-*g*-PEO and PAA-*g*-dodecyl, which were calculated by the method described in Section 3.3, against their concentration. It can be seen that the ζ-potential of PAA-*g*-PEO increased more rapidly than that of PAA. Moreover, as shown in Fig. 5, the ratio of effective charged monomers gradually increased with a decrease in concentration in regime I. These results indicate that more condensed counterions were gradually released in comparison with PAA during the process of dilution. This result cannot disregard the higher ζ-potential of PAA-*g*-PEO (in Fig. 6), which affected the binding capability of counterions with chains so that more counterions were released,[36] as shown in Fig. 7b. Moreover, the possible steric hindrance effect of PEO side chains also promoted the release of counterions. For PAA-*g*-dodecyl, we can see that the ζ-potential (Fig. 6) was lower. Moreover, the ratio of effective charged monomers gradually increased with a decrease in concentration (Fig. 5) in this regime. As illustrated in Fig. 7b, as the binding capability of counterions with chains was lower than that for PAA, the disintegration of inter- and intramolecular hydrophobic microdomains

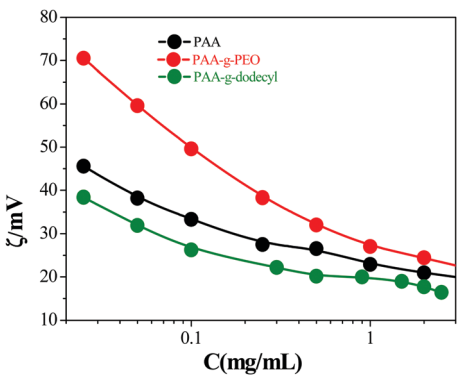


Fig. 6 The ζ-potential of PAA, PAA-*g*-PEO and PAA-*g*-dodecyl chains in aqueous solution as a function of their concentrations.

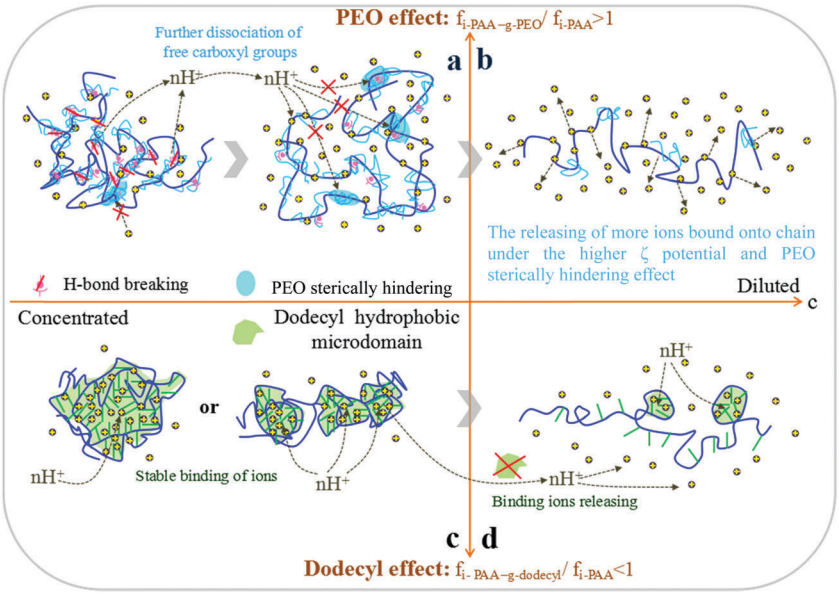


Fig. 7 Evolution of ionization properties of grafted PAA chains as affected by PEO (a and b) and dodecyl side chains (c and d) in solution from a concentrated to a dilute regime. PAA main chain molecules are indicated by dark blue lines, whereas PEO and dodecyl are represented by shallow blue and green lines, respectively. The yellow cross-shaped dots represent $H^+$ cations.

of dodecyl side chains in this regime led to the release of more counterions (Fig. 7d).

Furthermore, in order to reveal the coupling interactions between hydrophilic PEO and hydrophobic dodecyl side chains, we discussed the effective charges and ionization properties of PAA-*g*-PEO-*g*-dodecyl in aqueous solution over the concentration range of 0.0125 to 19.5 mg $mL^{-1}$. It is worth mentioning that we found both superposition and offsetting effects of PEO and dodecyl side chains (Fig. 5, dark yellow), which has never been reported in the literature. The superposition effect is evidenced by the trend in the evolution of $f_i/f_{i\text{-}PAA}$ with concentration for PAA, PAA-*g*-PEO and PAA-*g*-PEO-*g*-dodecyl in Fig. 5 (the red dashed arrow plus the green arrow make dark yellow). The offsetting effect is evidenced by the values of $f_i/f_{i\text{-}PAA}$ for PAA, PAA-*g*-PEO and PAA-*g*-PEO-*g*-dodecyl (the dark yellow line is between the red line and the green line). Moreover, it can be observed that the value of $f_{i\text{-}PAA\text{-}g\text{-}PEO\text{-}g\text{-}dodecyl}/f_{i\text{-}PAA}$ is closer to that of $f_{i\text{-}PAA\text{-}g\text{-}PEO}/f_{i\text{-}PAA}$, which is also consistent with the sample of PAA-*g*-PEO-*g*-dodecyl itself, which contained a higher fraction of dodecyl side chains ($f_{dodecyl} \approx 4.2\%$; $f_{PEO} \approx 0.53\%$).

**4.1.4 Mechanism of influence of side chains on conformation.** In Section 4.1.2, three concentration regimes, namely, dilute non-entanglement, semi-dilute non-entanglement and semi-dilute entanglement, were identified. In general, the contribution of association interactions induced by side chains to the overlapping and entanglement of PAA chains has been realized and is mentioned above.[12,16] Here, we further point out the role of ionization properties affected by side chains in the capability to overlap and undergo entanglement. In comparison with PAA, the higher effective charges owing to the presence of PEO side chains leads to higher overlapping capability and a wider non-entanglement regime as represented by $c^e/c^*$ for PAA-*g*-PEO. Furthermore, we can infer that the final increased entangling capability of PAA-*g*-PEO and overlapping capability of PAA-*g*-dodecyl (see Section 4.1.2) are mainly the results of association interactions among chains induced by side chains, not the fact that their effective charges are higher than those of PAA.

Fig. 8 shows the concentration dependence of the correlation length $\xi$ for PAA, PAA-*g*-PEO and PAA-*g*-dodecyl chains in solution determined by using the dielectric analysis method described in Section 3.3. With an increase in concentration, the correlation lengths $\xi$ of the three samples remained constant over the dilute concentration range below about 0.1 mg $mL^{-1}$ and then gradually decreased because of a strong electrical screening effect from the counterions from overlapping or entangled chains over the semi-dilute concentration range. From Fig. 8, it is also clearly seen that the correlation length of PAA-*g*-PEO was greater than that of PAA and the correlation

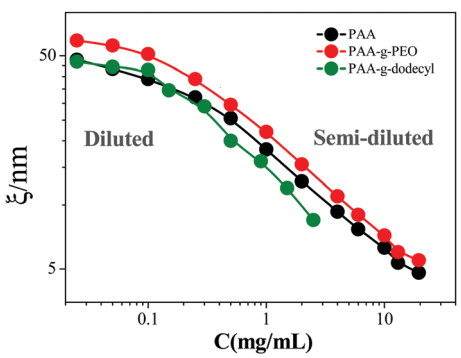


Fig. 8 Correlation lengths $\xi$ of PAA, PAA-*g*-PEO and PAA-*g*-dodecyl chains in aqueous solution as a function of their concentrations.

 

length of PAA-*g*-dodecyl was smaller than that of PAA over the entire concentration regime, which is consistent with the order of their effective charges determined in Section 4.1.3 ($f_{\text{i-PAA-}g\text{-PEO}} > f_{\text{i-PAA}} > f_{\text{i-PAA-}g\text{-dodecyl}}$).

This result strongly indicates that the consideration of electrical interactions is essential in discussing the effect of side chains on chain conformation, in addition to hydrogen bonding and hydrophobic interactions.

### 4.2 Effect of side chains on counterion distribution and fluctuation behavior in PAA

As shown in Fig. 2 and 3, the dependences on frequency and concentration of the dielectric constants ($\varepsilon$ and $\varepsilon''$) of PAA-*g*-PEO and PAA-*g*-dodecyl seem to be distinct from those for linear PAA. Notably, this trend also indicates that the counterion distribution and ion fluctuation around chains are possibly affected by side chains. In our work, the investigation of the counterion atmosphere by dielectric analysis with the DLP model (the method described in Section 2) enabled us to further study the possible role of side chains in counterion distribution and the dynamic properties of counterions around chains. Fig. 9a and b show the evolution of the linear density of counterions $\rho$ and the thickness of the electric double layer $\kappa^{-1}$ with concentration for the three samples. Interestingly, sudden increases in the linear density of counterions $\rho$ were found around the crossover concentration region (the first set of dashed lines) and the entanglement concentration region (the second set of dashed lines), which indicates that an overlap of the counterion atmospheres of different chains occurred around the crossover concentration region and was enhanced by the interpenetration and entanglement of chains. Moreover, the overlap of the counterion atmospheres also resulted in significant screening of the electrostatic potential between monomers, which then resulted in a decrease in the thickness of the electric double layer $\kappa^{-1}$.[45] We can therefore estimate the degree of overlap of counterion atmospheres or the counterion density within the EDL by the result for the $\kappa^{-1}$ value of the EDL. For PAA-*g*-PEO, we have found that there were more counterions around chains than for PAA (Section 4.1.3). The lower $\kappa^{-1}$ value above about 0.2 mg mL$^{-1}$ in Fig. 9b (red line) indicates that the degree of overlap of counterion atmospheres and the counterion density within the EDL were greater than for PAA. For PAA-*g*-dodecyl, there were fewer counterions around chains than for PAA (Section 4.1.3), and therefore the decrease in the value of $\kappa^{-1}$ should be slower than that for PAA. From Fig. 9b (green line), the slope of the decrease in the value of $\kappa^{-1}$ for PAA-*g*-dodecyl is similar to that for PAA, which also suggests that the degree of overlap of counterion atmospheres and the counterion density within the EDL were possibly greater than those for PAA.

As mentioned in Section 4.1.1, under the ac electric field the counterion flux was divided into fluctuations perpendicular to chains and along chains. Here, we only consider the first-order ion flux, which is high-frequency relaxation caused by ion fluctuations perpendicular to chains. According to the classical theory of ion fluctuations proposed by Ito and Hayakawa,[29] the relaxation time for this fluctuation is defined as follows:

$$\tau_{\text{h}} \sim \frac{L_{\text{i}}^2}{6D_{\text{i}}} \tag{19}$$

where $L$ is the distance of ion fluctuations perpendicular to polymer chains and $D_{\text{i}}$ is the corresponding diffusion rate constant. The relaxation increment is given by:

$$\Delta\varepsilon_{\text{h}} \sim f_{\text{i}} c \frac{\text{e}^2 L_{\text{i}}^2}{\varepsilon_0 k_{\text{B}} T} \tag{20}$$

Combining eqn (19) and (20) yields an expression for $D_{\text{i}}$:

$$D_{\text{i}} \sim \frac{k_{\text{B}} T \Delta\varepsilon_{\text{h}}}{6 f_{\text{i}} c_{\text{p}} \text{e}^2 \tau_{\text{h}}} \tag{21}$$

The ratios of the diffusion rate constants of counterions for PAA-*g*-PEO and PAA-*g*-dodecyl ($D_{\text{i}}$) to that for PAA ($D_{\text{i-PAA}}$) can therefore be expressed as:

$$\frac{D_{\text{i}}}{D_{\text{i-PAA}}} = \frac{f_{\text{i-PAA}} \Delta\varepsilon_{\text{h}} \tau_{\text{h-PAA}}}{f_{\text{i}} \tau_{\text{h}} \Delta\varepsilon_{\text{h-PAA}}} \tag{22}$$

Similarly, according to eqn (20), the ratio of the counterion fluctuation distance for PAA-*g*-PEO and PAA-*g*-dodecyl ($L_{\text{i}}$) in comparison with that for PAA ($L_{\text{i-PAA}}$) is given by:

$$\frac{L_{\text{i}}}{L_{\text{i-PAA}}} = \left( \frac{D_{\text{i}} \tau_{\text{h}}}{D_{\text{i-PAA}} \tau_{\text{h-PAA}}} \right)^{\frac{1}{2}} \tag{23}$$

According to eqn (22) and (23), the ratios of the rate constant ($D_{\text{i}}/D_{\text{i-PAA}}$) and distance of ion fluctuations perpendicular to

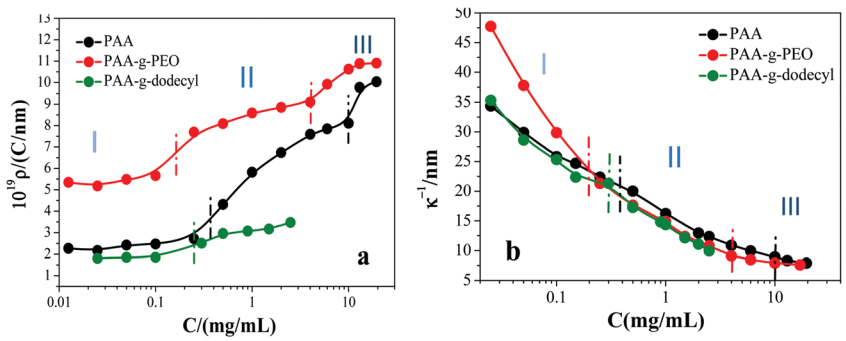


Fig. 9 Concentration dependence of the linear density of counterions $\rho$ (a) and the thickness of the electric double layer $\kappa^{-1}$ (b) for aqueous solutions of PAA, PAA-*g*-PEO, and PAA-*g*-dodecyl.

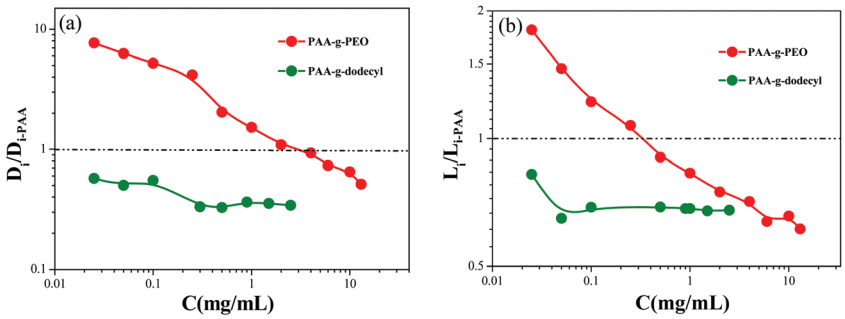


Fig. 10 Ratios of the rate constant (a) and distance of ion fluctuations perpendicular to polymer chains (b) for PAA-*g*-PEO and PAA-*g*-dodecyl to that for PAA in solution at different concentrations.

polymer chains ($L_i/L_{i\text{-PAA}}$) for PAA-*g*-PEO and PAA-*g*-dodecyl to that for PAA were calculated by substituting $f_i/f_{i\text{-PAA}}$ (Fig. 6) and the dielectric relaxation parameters $\Delta\varepsilon_h/\Delta\varepsilon_{h\text{-PAA}}$ and $\tau_h/\tau_{h\text{-PAA}}$ (Table 1), and the results are presented in Fig. 10. It can be seen from Fig. 10a that the rate constant for PAA-*g*-PEO was greater than that for PAA ($D_{i\text{-PAA-}g\text{-PEO}}/D_{i\text{-PAA}} > 1$) below 0.1 mg mL$^{-1}$ and then gradually approximated to that for PAA, even becoming lower than that for PAA with an increase in concentration. In contrast to PAA-*g*-PEO, the rate constant for PAA-*g*-dodecyl was lower than that for PAA over the entire concentration regime. The results for the effective charges (in Section 4.1.3) and electrostatic potential (Table 2) may be sufficient to explain this phenomenon. As shown in Fig. 5 and 6, the higher effective charges and electrostatic potential on PAA-*g*-PEO made the counterions fluctuate perpendicularly to chains more rapidly below 4 mg mL$^{-1}$. In the case of PAA-*g*-dodecyl, the opposite situation was the case. In theory, there is a proportional relationship between the ion fluctuation distance $L_i$ and the thickness of the electric double layer ($\kappa^{-1}$) around polymer chains, as follows:[34]

$$L_i \sim 2a_1\kappa^{-1} \quad (24)$$

where $a_1$ is a proportionality constant. The proportionality between $L_i$ and $\kappa^{-1}$ in eqn (24) was observed in our work, which gave higher values of $\kappa^{-1}$ and $L_i$ for PAA-*g*-PEO below 0.1 mg mL$^{-1}$ and, conversely, lower values of $\kappa^{-1}$ and $L_i$ above 0.1 mg mL$^{-1}$ (red lines in Fig. 9b and 10b). Besides, this proportionality was also found for PAA-*g*-dodecyl, which exhibited lower values of $\kappa^{-1}$ and $L_i$ than PAA (green lines in Fig. 9b and 10b).

## 5. Conclusions

In this work, we clarified the nature of the effects of side chains on chain conformation and the distribution and fluctuation of counterions around chains in detail by dielectric spectroscopy. Double dielectric relaxations were observed for aqueous solutions of PAA, PAA-*g*-PEO and PAA-*g*-dodecyl over radio frequency ranges. A double-layer polarization model is well suited to the analysis of these two relaxations, and several valuable conformational and electrokinetic parameters were determined. The concentration dependences of the dielectric increment and relaxation time exhibited two abrupt changes, which were confirmed to correspond to the crossover concentration and entanglement concentration, respectively. It was shown that PEO and dodecyl side chains had significant influences on the overlapping and entanglement of chains. The ratio of effective charges of PAA-*g*-PEO or PAA-*g*-dodecyl, which was calculated from conductivity data, showed an increase in effective charges due to PEO side chains and a decrease in effective charges due to dodecyl side chains. It was suggested that the steric hindrance effect of PEO side chains and the counterion binding effect of dodecyl side chains played important roles in these changes in effective charges or ionization properties. Moreover, coupling interactions of mutual superposition and offsetting between PEO and dodecyl side chains were observed.

Determination of the correlation length by dielectric analysis showed that PAA-*g*-PEO molecules are more stretched than PAA molecules and PAA-*g*-dodecyl molecules are more contracted than PAA molecules. The linear density of counterions and the thickness of the electric double layer (EDL) around chains suggest that the degree of interpenetration of the EDL for PAA-*g*-PEO and PAA-*g*-dodecyl was higher than that for PAA. In addition, the rate constant ratio and distance of first-order flux estimated by the theory of counterion fluctuations show that counterion fluctuations in PAA are strongly affected by PEO and dodecyl side chains. It has been demonstrated that changes in the effective charges or ionization properties play an important role in the effect of side chains on chain conformation and the distribution and dynamics of counterions and cannot be ignored. These findings not only contribute to an understanding of the effect of side chains on the structure and properties of polyelectrolytes in solution, but also show the advantages and potential of dielectric spectroscopy for evaluating the physicochemical properties of flexible PEs.

## Acknowledgements

The authors gratefully wish to thank Prof. Charles C. Han and Dr Jin-kun Hao (Institute of Chemistry, Chinese Academy of Sciences, China) for supplying the sample used in this experiment. This work was supported by financial support from the National Natural Science Foundation of China

 

(No. 21173025, 21473012) and the Major Research Plan of NSFC (No. 21233003).

## References


1 J. Bohrisch, C. D. Eisenbach and W. Jaeger, New Polyelectrolyte Architectures, Polyelectrolytes with Defined Molecular Architecture I, *Adv. Polym. Sci.*, 2004, **165**, 3–15.

2 M. A. Winnik and A. Yekta, Associative polymers in aqueous solution, *Curr. Opin. Colloid Interface Sci.*, 1997, **2**(4), 424–436.

3 A. V. Dobrynin and M. Rubinstein, Theory of polyelectrolytes in solutions and at surfaces, *Prog. Polym. Sci.*, 2005, **30**, 1049–1118.

4 S. Alejandro and R. Maya Menaker, Polymeric micelles in mucosal drug delivery: challenges towards clinical translation, *Biotechnol. Adv.*, 2015, **33**(6), 1380–1392.

5 D. N. Schultz and J. E. Glass, *ACS Symposium Series: Polymers as Rheology Modifiers*, American Chemical Society, Washington, DC, 1991, p. 157–173.

6 K. Claus-Peter, H. Sven and S. Hannah, Adsorption of Poly(Acrylic Acid)-*graft*-Poly(Ethylene Glycol) on Polyelectrolyte Multilayers, *Prog. Colloid Polym. Sci.*, 2011, **138**, 95–101.

7 Y. Rouault and O. V. Borisov, Comb-Branched Polymers: Monte Carlo Simulation and Scaling, *Macromolecules*, 1996, **29**, 2605–2611.

8 W. Y. Liu, Y. J. Liu, G. S. Zeng, R. G. Liu and Y. Huang, Coil-to-rod conformational transition and single chain structure of graft copolymer by tuning the graft density, *Polymer*, 2012, **53**, 1005–1014.

9 A. Goodwin, S. Bobade, N.-G. Kang, D. Baskaran, K. L. Hong and J. Mays, Poly(styrene-*graft*-hyperbranched polyglycidol):synthesis and solution behavior of a hyperbranched polyelectrolyte, *RSC Adv.*, 2015, **5**, 5611–5616.

10 L. S. Zhang, J. P. Lin and S. L. Lin, Effect of Molecular Architecture on Phase Behavior of Graft Copolymers, *J. Phys. Chem. B*, 2008, **112**, 9720–9728.

11 F.-Q. Daniel, A.-M. Waldo M, G.-G. Álvaro and V.-L. Blanca, Conformational study on the thermal transition of chitosan-*g*-poly(*N*-vinylcaprolactam) in aqueous solution, *Colloid Polym. Sci.*, 2016, **294**, 555–563.

12 J. L. Li and K. S. Zhao, Effect of Side-Chain on Conformation of Poly(acrylic acid) and Its Dielectric Behaviors in Aqueous Solution: Hydrophobic and Hydrogen-Bonding Interactions and Mechanism of Relaxations, *J. Phys. Chem. B*, 2013, **117**, 11843–11852.

13 V. Andrey and M. Rubinstein, Counterion Condensation and Phase Separation in Solutions of Hydrophobic Polyelectrolytes, *Macromolecules*, 2001, **34**, 1964–1972.

14 J. Klier, A. B. Scranton and N. A. Peppas, Self-associating networks of poly(methacrylic acid-*g*-ethylene glycol), *Macromolecules*, 1990, **23**, 4944–4949.

15 S. Paillet, B. Grass, A. Khoukh, M. Torres, J. Desbrieres and A. J. Alejandro, *Macromolecules*, 2009, **42**, 4914–4917.

16 J. K. Hao, Z. Y. Li, H. Cheng, C. Wu and C. C. Han, Kinetically Driven Intra- and Interchain Association of Hydrophobically and Hydrophilically Modified Poly(acrylic acid) in Dilute Aqueous Solutions, *Macromolecules*, 2010, **43**, 9534–9540.

17 D. P. Garrett, L. J. William, W. S. Charles and L. M. Charles, Enhanced Coil Expansion and Intrapolymer Complex Formation of Linear Poly(methacrylic acid) Containing Poly(ethylene glycol) Grafts, *Macromolecules*, 2004, **37**, 2603–2612.

18 K. Benmansour, A. Mansri and J. Francois, Oligo(ethylene oxide) side-chain steric screening effects on conductimetric properties of grafted poly(4-vinylpyridinium) salts in aqueous solutions, *Polym. Int.*, 2003, **52**, 1506–1514.

19 J. Weber, V. Boyko and K. F. Arndt, Influence of Grafting on the Solution Properties and the Dissociation Behavior of Ionic/Nonionic Grafted Copolymers, *Macromol. Chem. Phys.*, 2007, **208**, 643–650.

20 K. Chandrasekar and G. Baskar, *J. Polym. Sci., Part A: Polym. Chem.*, 2006, **44**, 314–324.

21 W. Essafi, F. Lafuma and C. E. Williams, Anomalous counterion condensation in salt-free hydrophobic polyelectrolyte solutions: osmotic pressure measurements, *Europhys. Lett.*, 2005, **71**(6), 938–944.

22 V. M. Prabhu, Counterion structure and dynamics in polyelectrolyte solution, *Curr. Opin. Colloid Interface Sci.*, 2005, **10**, 2–8.

23 U. Scheler, NMR on polyelectrolytes, *Curr. Opin. Colloid Interface Sci.*, 2009, **14**, 212–215.

24 F. Bordi, C. Cametti and R. H. Colby, Dielectric spectroscopy and conductivity of polyelectrolyte solutions, *J. Phys.: Condens. Matter*, 2004, **16**, R1423–R1463.

25 F. Bordi, C. Cametti and G. Paradoss, Conformation transitions in aqueous solutions of poly(L-glutamic acid): a radiowave dielectric study, *J. Phys. Chem.*, 1992, **96**, 8194–8200.

26 D. Truzzolillo, C. Cametti and S. Sennatoab, Dielectric properties of differently flexible polyions: a scaling approach, *Phys. Chem. Chem. Phys.*, 2009, **11**, 1780–1786.

27 T. Sato, H. Sakai, K. Sou, R. Buchner and E. Tsuchida, Poly(ethylene glycol)-conjugated phospholipids in aqueous micellar solutions: hydration, static structure, and interparticle interactions, *J. Phys. Chem. B*, 2007, **111**, 1393–1401.

28 F. Van Der Touw and M. Mandel, Dielectric increment and dielectric dispersion of solutions containing simple charged linear macromolecules: I. Theory, *Biophys. Chem.*, 1974, **2**, 218–230.

29 K. Ito and R. Hayakawa, Crossover behavior in high-frequency dielectric relaxation of linear polyions in dilute and semidilute solutions, *Macromolecules*, 1990, **23**, 857–862.

30 T. Mitsumata, T. Miura, N. Takahashi and M. Kawai, Ionic state and chain conformation for aqueous solutions of supergiant cyanobacterial polysaccharide, *Phys. Rev. E: Stat., Nonlinear, Soft Matter Phys.*, 2013, **87**, 042607.

31 J. L. Li and K. S. Zhao, The chain conformation and relaxation dynamics of poly(acrylic acid)-*graft*-poly(ethylene oxide)-*graft*-dodecyl in water: effect of side-chains and distribution of counterions, *Phys. Chem. Chem. Phys.*, 2015, **17**, 4175.

32 C. Y. David Lu, Theory of the polyelectrolyte dielectric function, *Phys. Rev. E: Stat., Nonlinear, Soft Matter Phys.*, 2011, **84**, 041804.

33 S. Takashima, Dielectric Dispersion of Deoxyribonucleic Acid II, *J. Phys. Chem.*, 1966, **70**, 1372–1380.
34 Y. Katsumoto, S. Omori, D. Yamamoto, A. Yasuda and K. Asami, Dielectric dispersion of short single-stranded DNA in aqueous solutions with and without added salt, *Phys. Rev. E: Stat., Nonlinear, Soft Matter Phys.*, 2007, **75**, 011911.
35 M. Fixman, Charged macromolecules in external fields. I. The sphere, *J. Chem. Phys.*, 1980, **72**, 5177–5186.
36 M. Yokoyama, T. Okano, Y. Sakurai, A. Kikuchi, N. Ohsako, Y. Nagasaki and K. Kataoka, Synthesis of poly(ethylene oxide) with heterobifunctional reactive groups at its terminals by an anionic initiator, *Bioconjugate Chem.*, 1992, **3**, 275.
37 H. Schwan, Determination of biological impedances, in *Physical Techniques in Biological Research*, ed. W. L. Nastuk, Academic Press, Inc., New York, 1963.
38 S. Forster and M. Schmidt, Polyelectrolytes in solution. Springer, *Adv. Polym. Sci.*, 1995, **120**, 51–133.
39 G. Jérémie, C. Fabrice and B. François, Structure Transition in PSS/Lysozyme Complexes: A Chain-Conformation-Driven Process, as Directly Seen by Small Angle Neutron Scattering, *Macromolecules*, 2008, **41**, 2898–2907.
40 R. Dirk, M. Beate, M. P. Florian and W. Simone, How does the chain extension of poly(acrylic acid) scale in aqueous solution? A combined study with light scattering and computer simulation, *J. Chem. Phys.*, 2002, **116**(20), 9100.
41 E. A. Litmanovich, O. Z. Svetlana and V. S. Georgi, Influence of Chain Charge and Complexation on the Overlap and Entanglements Formation in Poly(acrylic acid) Salt-Containing Aqueous Solutions, *J. Phys. Chem. B*, 2007, **111**, 8567–8571.
42 M. Ye, D. Zhang, L. Han, T. Jonathon and O. Christine, Synthesis, preparation, and conformation of stimulus-responsive end-grafted poly(methacrylic acid-*g*-ethylene glycol) layers, *Soft Matter*, 2006, **2**, 243–256.
43 K. Denavand and J. C. Selser, Polyethylene oxide does not necessarily aggregate in water, *Nature*, 1990, **343**, 739–741.
44 A. Benkhira, E. Franta and E. François, Conformation of Poly(l,3-dioxolane) in Dilute and Semidilute Aqueous Solutions, *Macromolecules*, 1994, **27**, 3963.
45 M. Cranfeldt and B. Jonsson, A Mean-Field Monte Carlo Technique for Studies of Electric Double Layers and Flexible Polyelectrolytes, *J. Phys. Chem.*, 1992, **96**(24), 10080–10086.

 